Biorenewable and circular polydiketoenamine plastics

Jeremy Demarteau[1], Benjamin Cousineau[1], Zilong Wang[2–5], Baishakhi Bose[5], Seokjung Cheong[2–5], Guangxu Lan [2,5], Nawa R. Baral[2,5], Simon J. Teat[6], Corinne D. Scown[2,5,7,8], Jay D. Keasling[2–5,9,10] , Brett A. Helms[1,2,11,*]

[1]The Molecular Foundry, Lawrence Berkeley National Laboratory, Berkeley, CA 94720 USA.

[2]Joint BioEnergy Institute, Emeryville, California 94608 USA.

[3]Department of Chemical and Biomolecular Engineering & Department of Bioengineering, University of California, Berkeley, California 94720 USA.

[4]QB3 Institute, University of California, Berkeley, California 94720, USA.

[5]Biological Systems and Engineering Division, Lawrence Berkeley National Laboratory, Berkeley, California 94720 USA.

[6]Advanced Light Source, Lawrence Berkeley National Laboratory, Berkeley, CA 94720 USA.

[7]Energy Analysis and Environmental Impacts Division, Lawrence Berkeley National Laboratory, Berkeley, California 94720, United States

[8]Energy & Biosciences Institute, University of California, Berkeley, California 94720 USA

[9]Center for Synthetic Biochemistry, Shenzhen Institutes for Advanced Technologies, Shenzhen 518055, P.R. China

[10]The Novo Nordisk Foundation Center for Biosustainability, Technical University Denmark, Kemitorvet, Building 220, Kongens Lyngby 2800, Denmark

[11]Materials Sciences Division, Lawrence Berkeley National Laboratory, Berkeley, CA 94720 USA.

*Correspondence: bahelms@lbl.gov

Abstract

Amid growing concerns over the human health and environmental impacts of plastic waste, the most promising solution would be to build a circular plastics economy where sustainability considerations dictate the full life cycle of plastics use including replacing petrochemicals with biorenewables. Here, we show that by incorporating the polyketide triacetic acid lactone (TAL) in polydiketoenamines (PDK), we increase the working temperature of these circular plastics, opening the door wider to applications where circularity is urgently needed. By varying the number of carbons of TAL-derived monomers, both polymer properties and recycling efficiency are affected. Simply using glucose as the main carbon source, we engineered a process for producing bioTAL under fed-batch fermentation. A systems analysis of this bioprocess at different scenarios quantifies the environmental and economic benefits of PDK plastics and the risks when implemented at an industrial scale, providing opportunities in biorenewable circularity.

Main Text

Bringing biorenewable circularity to plastics is critical to ensuring their sustainability.[1–3] While bio-based monomers used to produce plastic resins are increasingly available from biomass and bioproducts,[1,4,5] using them simply as drop-in replacements for commodity petrochemicals fails to deliver a bio-advantage in performance.[6] Justifying their use in plastics production therefore remains difficult, as they are often produced at higher cost than the petrochemical they seek to replace. Furthermore, few existing plastics, even if produced from bio-monomers, are chemically recycled in closed loops, particularly monomer-to-monomer.[1,7] Without biorenewable circularity, we will continue to consume the dwindling supply of fossil resources to meet the rapidly growing demand for plastics;[8] moreover, we will have few incentives to recover plastic waste for recycling and reuse, failing to meet our goals for sustainable manufacturing. Future generations of plastics should emphasize bio-advantaged designs that achieve high efficiency in chemical recycling with respect to monomer recovery at end of life,[6,9] so that the biorenewable content may be recirculated across the maximum possible number of manufacturing cycles. If this were realized, there could be a confluence of performance, manufacturing, and economic benefits to motivate the switch to new materials in the transition to a circular bio-plastics economy.

In support of this paradigm shift, we and others have demonstrated circularity in emerging bio-plastics is achievable through co-design of polymers and chemical recycling processes (e.g., acidolysis, solvolysis, enzymolysis, and catalytic ring-closing depolymerization).[10–28] Chen *et al.* have exploited ring–chain equilibria to enable circularity in polyesters and nylons from strained lactone and lactam monomers, some of which can be produced from bio-based raw materials.[13–15] Complementing these efforts, Mecking *et al.* have prioritized solvolysis in the deconstruction of polyesters and polycarbonates from high molecular weight diols and carboxylic acids.[10] Solvolysis and acidolysis are likewise applicable to bio-plastics featuring imine and diketoenamine bonds. Some of these bio-plastics have even shown properties similar to petroleum-derived plastics that remain difficult to recycle in closed-loops, such as polyethylene and polyurethane.[10] Among them, bio-plastics based on polydiketoenamine (PDK) stand out for the concomitantly high efficiency and low cost required to chemically recycle them to the same monomers used in primary resin

production.[23–28] Yet, it remains a significant challenge to demonstrate circularity in bio-plastics, while deriving benefits from their constituent bio-monomers.

Here, we show that biorenewable circularity in plastics concomitantly delivers a useful bio-advantage by incorporating the polyketide triacetic lactone (TAL) in polydiketoenamines (PDK), which are deconstructed to monomer at end of life with low carbon intensity in high yield and purity. The bio-advantage of TAL arises from its planarity, which promotes efficient stacking in the solid state and has the effect of densifying TAL-based PDKs (TAL-PDK). This densification raises the glass transition temperature (T_g) beyond a key threshold of 150 °C, making possible the use of TAL-PDKs in broader applications (e.g., automotive),[29] where structural integrity up to that temperature is of great importance. To understand the prospects for producing PDK resins from TAL, we developed a fed-batch fermentation process for bioTAL production using an engineered strain of *E. coli* that expresses a heterologous polyketoacyl-CoA thiolase, BktB, which converts acetyl-CoA into TAL in high titer. We also provide a detailed systems analysis of this process at different production volumes, where the environmental and economic benefits derived from biorenewability are quantified and delineated in the context of managing risk along the path to producing bioTAL and TAL-PDK resins at industrial scale.

Results

Biorenewable Triacetic Acid Lactone-based PDK Resins

PDK resins are prepared via spontaneous "click" polycondensation reactions between polytopic triketone and amine monomers; no chemical condensation agent is required and water is the sole by-product of the reaction.[23–28] Triketone monomers used in PDK production are synthesized from various 1,3-diketones and diacids. During synthesis, acylation of the 1,3-diketone typically occurs first at oxygen, which is then followed by an *O*- to *C*-acyl rearrangement catalyzed by 4-(dimethylamino)pyridine (DMAP).[26] Owing to structural similarities between *O*-acyl intermediates and the likely reactivity of the preferred tautomer of TAL, we hypothesized that TAL could stand in place of conventional petrochemical 1,3-diketones, such as dimedone, in monomer synthesis alongside common aliphatic $C_{8–12}$ dicarboxylic acids (**Fig. 1a**) to make available biorenewable triketone monomers (TAL-TK **1**–**5**) and in turn PDK resins (TAL-PDK **1**–**5**). Confirming this hypothesis, TAL-TK **1**–**5** were prepared in 40–63% yield (after recrystallization) using *N*,*N'*-dicyclohexylcarbodiimide (DCC) and DMAP. We obtained single-crystal X-ray structures for TAL-TK **1**, **3**, and **5**—all of which evidenced herring-bone packing of the monomers in the solid-state, due to stacking enabled by the planarity of TAL (**Fig. 1b & Supplementary Figs. 1–2**). This propensity for stacking and densification is highly differentiated from that exhibited by a similar triketone monomer prepared from the petrochemical dimedone, which is not planar (**Supplementary Table 1**). This difference in crystallinity is further exemplified in DSC analysis of TAL-TK monomers, showing sharp endothermic melting peaks for TAL-TKs **1**, **3** and **5** (150, 143 and 143 °C, respectively), while TAL-TKs **2** and **4** shows broader transitions at lower temperatures (60 and 100 °C, respectively) (**Supplementary Fig. 3)**. It follows that the properties of PDK resins produced from these triketone monomers may likewise have different properties arising from the unique microstructures afforded to each.

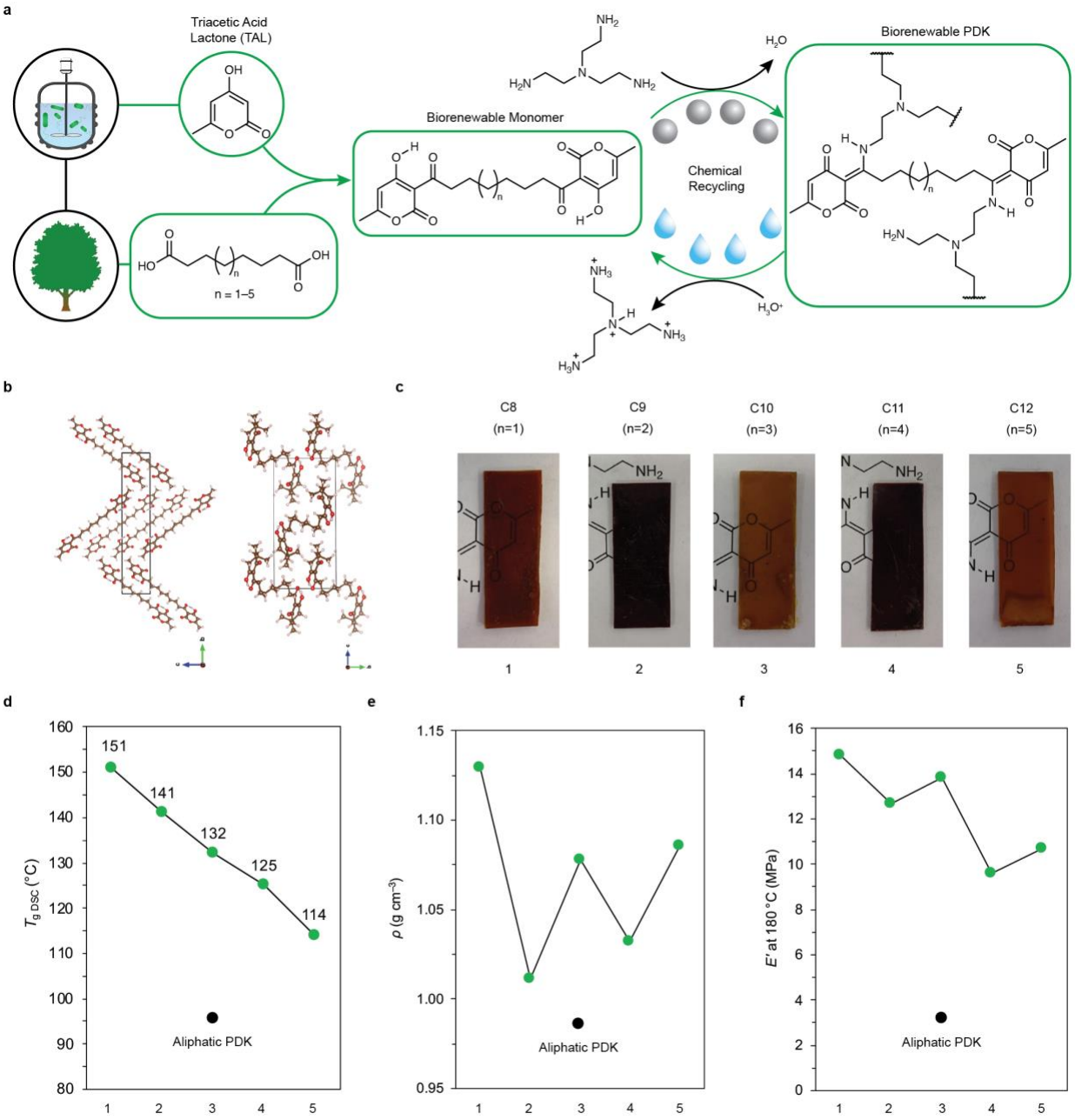

Fig. 1: Biorenewable circularity in PDK plastics derived from triacetic acid lactone (TAL). **a**, Synthesis and chemical recycling of biorenewable PDK resins derived from TAL (TAL-PDKs **1**–**5**). **b**, Single-crystal X-ray structures of triketone TAL-TK **3** (top) and a related aliphatic triketone prepared from the petrochemical dimedone in place of TAL (bottom). **c**, Compression-molded samples of TAL-PDKs **1–5**. **d**, Glass transition temperatures (T_g) measured by DSC for TAL-PDK **1–5** and a related aliphatic PDK resin prepared from dimedone. **e**, Density and **f**, storage modulus (at rubbery state, 180 °C) of compression-molded TAL-PDK **1–5** and a related aliphatic PDK prepared from dimedone.

To understand these emergent microstructure–property relationships, we first prepared TAL-PDK resins **1**–**5** from TAL-TK monomers **1**–**5** and *tris*(2-aminoethyl)amine (TREN); as a control, we

also prepared a PDK resin from TREN and a triketone monomer derived from dimedone. To confirm that the polycondensation was complete, we performed ^{13}C solid-state nuclear magnetic resonance (^{13}C SSNMR) spectroscopy on powdered samples of TAL-PDK **1**–**5** (**Supplementary Figs. 4–8**). We observed a disappearance of sharp peaks, otherwise corresponding to the crystalline triketone monomer, as well as a concomitant broadening of peaks corresponding to the polymer network. We further confirmed the extent of polymerization was high by powder X-ray diffraction (PXRD), where sharp and intense peaks associated with the Bragg reflections of crystalline triketone monomers completely subsided to peaks exhibiting lower-intensity and significant broadening due to amorphization into a glassy vitrimer network (**Supplementary Fig. 9**).

Enabled by the intrinsic dynamic covalent character of vitrimers, crosslinked PDK resin powders remain thermally processable, e.g., by compression molding.[30–32] For TAL-PDK resins **1**–**5**, compression molding at 20 kPsi pressure required temperatures of 150, 140, 130, 125, and 110 °C, respectively, to fabricate samples (**Fig. 1c**; **Supplementary Fig. 10**); thus, lowering vitrimer crosslinking density has the effect of lowering the energy requirement for PDK manufacturing. Whereas the expected color and high transparency of the vitrimers were readily apparent for TAL-PDK **1**, **3**, and **5** (as well as the control), colors were unexpectedly darker and hazier for TAL-PDK **2** and **4**. The natural hue of TAL-PDK resins, which varies with crosslinking density and odd–even effects, would need to be accounted for in compounding with pigments to arrive at desired specifications. Nonetheless, we observed a monotonic and well-behaved decrease in the glass transition temperature (T_g) with decreasing crosslinking density (**Fig. 1d**; **Supplementary Fig. 11**). Importantly, in all cases, we found that TAL dramatically raises T_g when incorporated into PDK resins: for example, the T_g of biorenewable TAL-PDK **3** is 36 °C higher than that of the related dimedone petrochemical control (T_g = 96 °C), pointing to the key role of PDK microstructure on thermal properties. To provide context for thermal stability, thermal gravimetric analysis (TGA) data of the different formulations, with monomers (TAL-TK **1**–**5**), powder and pressed-molded polymers (TAL-PDK **1**–**5**) do not show any degradation below 200 °C (**Supplementary Fig. 12**). Structural integrity of glassy polymer networks is critical for most commercial applications, from automotive to protective barriers and sporting gear; increasing T_g to meet product specifications remains an outstanding challenge, yet appears addressable with TAL-based PDK resins on account of their unique microstructure.

Motivated by this bio-advantage and its link to polymer microstructure, we carried out further studies of PDK properties, where microstructure often dictates outcomes, including density (ρ) and storage modulus (E') at temperatures above T_g. For elastic polymer networks, E' is proportional to ρ as well as the crosslinking density. Absent significant changes to ρ (which are rare), E' should decrease monotonically with decreasing crosslinking density, as was observed for T_g; however, that is not what we observed experimentally. Instead, we observed odd–even effects in both ρ and E', depending on the length of the diacid incorporated into the TAL-derived triketone monomer (**Fig. 1e–f**; **Supplementary Fig. 13**). In all cases, ρ and E' were higher for TAL-PDK materials than those of the related dimedone petrochemical control (**Supplementary Tables 2 & 3**), consistent with the body of evidence presented herein, indicating more efficient packing in the solid-state and useful gains in elasticity and stiffness. For example, ρ is 1.078 g cm^{-3} and E' is 13.5 MPa for TAL-PDK **3**, whereas ρ is 0.987 g cm^{-3} and E' is only 3.5 MPa for the control (i.e., 3.9-fold lower than TAL-PDK **3**). We are unaware of previous reports of odd–even effects in vitrimer microstructure–property relationships, yet they appear intrinsic and relevant to their design for

function. Until now, odd–even effects in elastic polymer networks had only been explored theoretically, e.g., with respect to monomer topology, accounting for number of networking functionality in the monomers.[33] Now, molecular configuration of constituent monomers and their influence on polymer chain conformation within the network architecture emerge as further points of interest and intrigue. Though unrelated, given the dissimilarity between linear and crosslinked polymer architectures, these observations are nonetheless reminiscent of odd–even effects in thermal properties of thermoplastics, e.g., the melting points of 1,*n*-nylons.[34] Odd–Even effects, observed here in TAL-PDK materials, may be universal for polymer networks. In this way, we continue to unravel the foundations of thermoplastic-like character of vitrimers,[30–32] including biorenewable PDK resins produced from TAL.

Molecular Basis for TAL-PDK Circularity in Recycling

PDK resins typically undergo deconstruction to triketone and amine monomers in strong acid at ambient temperature. Unlike triketone monomers derived from dimedone (i.e., the control), which have no cleavable linkages, those derived from TAL have motifs, such as the lactone, that may be susceptible to acidolysis. If lactone acidolysis is competitive with diketoenamine hydrolysis, then it could affect the materials efficiency of chemically recycling TAL-PDK resins back to monomer, e.g., if products other than TK **1**–**5** are also generated. To quantify the efficiency of circularity for TAL-PDK **1**–**5**, we carried out their acidolysis in 5 M HCl for 24 h, after which all deconstructed to dispersed solids of TAL-TK **1**–**5**, along with ionized TREN, which remained ionized in solution. We isolated TAL-TK **1**–**5** solids in 72, 93, 90, 98 and 100% yield, respectively (**Fig. 2c**); TREN can be recovered separately in high purity from the aqueous phase using a basic ion exchange resin.[23] Recycled TAL-TK **1**–**5** were indistinguishable from the pristine monomers by ^{1}H NMR spectroscopy (**Fig. 2b** and **Supplementary Figs. 14–18**), indicating that the TAL-TK motif is remarkably stable under these conditions. Furthermore, when compared to yields and purity for monomer recovery for dimedone-based PDK resins (i.e., derived from petrochemicals), TAL-PDK circularity compares favorably, particularly for resins with lower crosslinking density.

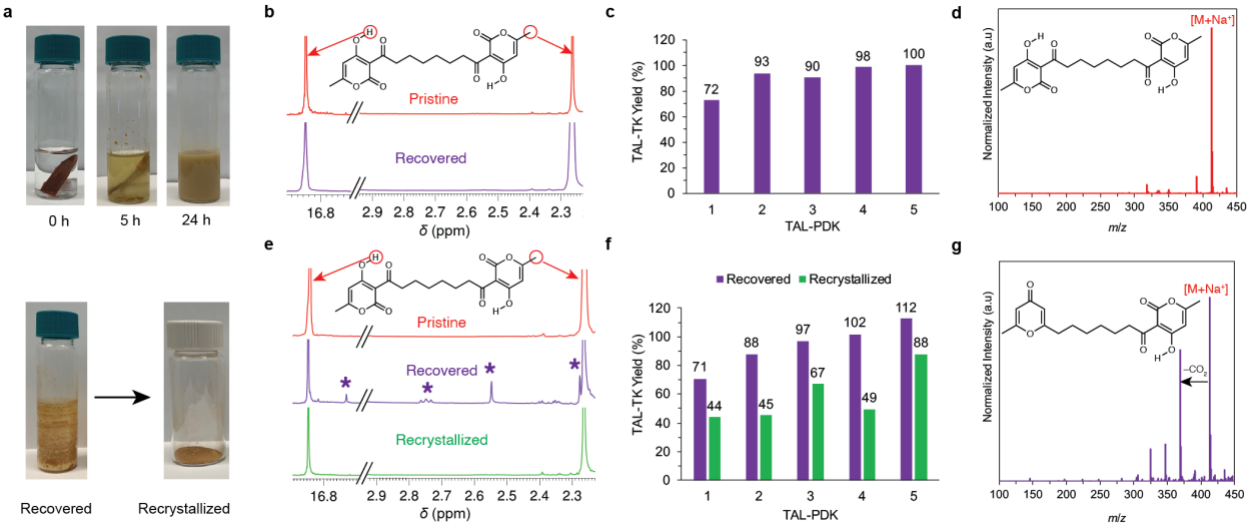

Fig. 2: Recycling of TAL-PDK formulations. a, Acid-catalyzed depolymerization of TAL-PDK **1** plastic and recovery of TAL-TK **1** monomer. **b**, ^{1}H NMR spectra of pristine TAL-TK **1** (*top*) along with crude TAL-TK **1** recovered from chemically-recycled TAL-PDK **1** resin (*bottom*). **c**,

TAK-TK yields after acidolysis of TAL-PDK resins. **d**, ESI-MS spectrum of TAL-TK **1**. **e**, ^{1}H NMR spectra of pristine TAL-TK **1** (*top*), crude TAL-TK **1** recovered after acidolysis of thermally-processed TAL-PDK **1** (*middle*), and TAL-TK **1** recovered from the crude after recrystallization in EtOH (*bottom*). Characteristic peaks in the ^{1}H NMR spectra for important structural motifs are highlighted with red arrows, while impurities are identified by using purple asterisks (*). **f**, TAL-TK yields for both crude (*purple*) and recrystallized (*green*) monomers after acidolysis of TAL-PDK plastics. **g**, ESI-MS spectrum of crude TAL-TK **1** recovered after acidolysis of thermally-processed TAK-PDK **1**.

In quantifying further the efficiency of TAL-PDK circularity in compression-molded samples, we likewise found that lowering the crosslinking density was useful for ensuring high monomer recovery from TAL-PDK resins that had undergone conversion to various form-factors at high pressure and temperature (**Fig. 2e & f** and **Supplementary Figs 19–32**). Polymer degradation during thermal processing during manufacturing or even mechanical recycling at end of life can be detrimental towards the development of circular plastics. An analysis of the degradation products formed after thermal processing can be informative towards an improved understanding of vulnerable structures and degradation pathways. These insights may provide new design criteria for constructing PDKs and other circular materials. To this end, we analyzed mass spectra for all crude triketones obtained after TAL-PDK deconstruction and compared these data with spectra obtained from the pristine monomers. In all cases, we observed a new and unique peak ~44 mass units below the peak corresponding to a $[\text{TAL-TK} + \text{Na}]^{+}$ ion (**Fig. 2d & g** and **Supplementary Figs. 28–32**). This indicated a loss of carbon dioxide from some monomers recovered after depolymerization. In parallel, we observed new yet minor peaks (<15%) in the δ = 16.7–17.0 ppm region of the ^{1}H NMR spectra for crude triketones. This indicated that while one triketone motif in the ditopic monomer remained intact in the minor byproduct of depolymerization reaction, the other had undergone decarboxylation during thermal processing (**Supplementary Figs. 19–27**). To remain consistent with the structural analysis afforded by mass spectrometry, it is likely this transformation generates a γ-pyrone. In cases where processing at high temperature and pressure led to materials degradation, we found triketone recrystallization from ethanol quite effective at removing unwanted γ-pyrone byproducts. Even with this additional purification process in place, TAL-TK **5** yields as high as 88% could be maintained, whereas in the absence of thermal processing and recrystallization, 100% yields were obtained. This understanding of the molecular basis for biorenewable circularity with TAL-PDK materials elevates future designs that benefit from lower crosslinking density to minimize mechanochemical activation of susceptible bonds within the TAL-PDK network.

Bioproduction of TAL

Polyketide natural products are ubiquitous: some serve as important medicines, while others as useful chemicals or feedstocks for materials.[35] TAL can be produced by the enzyme 2-pyrone synthase (2-PS), which catalyzes a succession of decarboxylative Claisen condensation reactions. TAL bioproduction with 2-PS has been achieved in *Yarrowia lipolytica* (36 g L^{-1}) and *Rhodotorula toruloides* (28 g L^{-1}), however overall yields from common carbon sources, such as glucose, could be improved if TAL synthases that perform non-decarboxylative Claisen condensation using acetyl-CoA as a substrate were used rather than those that perform decarboxylative condensation

using malonyl-CoA as a substrate.[36–38] Here, we used the non-decarboxylative polyketoacyl-CoA thiolase, BktB,[39] for TAL bioproduction in an engineered strain, *E. coli* JBEI-3695 (**Fig. 3a**). If successful, the advance could open the door to directly converting sugars from plant biomass hydrolysates to this valuable bioproduct in high yield,[40] closer to bringing biorenewable circularity to PDK resins.

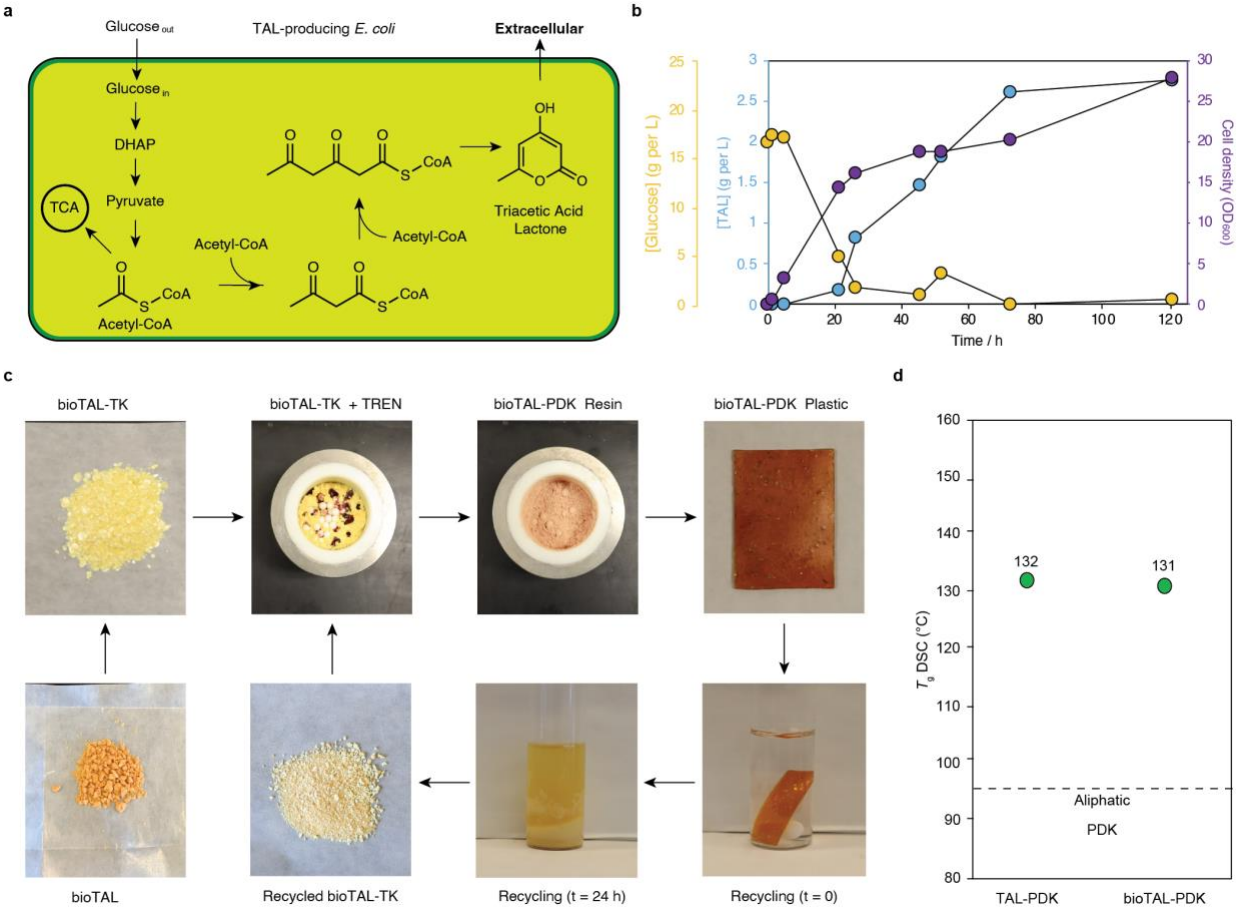

Fig. 3: Biosynthesis of triacetic acid lactone (bioTAL) and biorenewable TAL-PDK characterization. a, Metabolic pathway for TAL biosynthesis in engineered *E. coli* JBEI-3695. **b**, Cell growth (OD_{600}), TAL titer, and glucose concentration in the 1-L fed-batch fermentation using *E. coli* JBEI-3695 pBbA5A-BktB. **c**, Closed-loop production and chemical recycling of biorenewable TAL-PDK **3**. **d**, Comparison of glass transition temperatures for petrochemical and biorenewable TAL-PDK **3**, as well as a similar aliphatic PDK material produced from dimedone in place of BioTAL. Abbreviations: TCA, tricarboxylic acid cycle; DHAP, dihydroxyacetone phosphate.

We synthesized the gene encoding BktB from *Burkholderia sp.* RF2-non_BP3 with codon-optimization for *E. coli* and cloned it into the vector pBbA5A, followed by transformation into *E. coli* JBEI-3695, which had some of its mixed-acid production enzyme genes deleted (*ΔadhE ΔldhA ΔfrdBC* Δ*pta*) to enhance TAL production. We performed growth and production in a 1-L fed-batch bioreactor with optimized production media (**Supplementary Table 7**), using glucose as the main carbon source. We monitored cell growth using optical density at 600 nm (OD_{600}) of 1-mL cell samples removed periodically during the production. The cells achieved a final OD_{600} of 27.9

in 120 h and produced TAL to a final titer of 2.77 g L^{-1} (**Fig. 3b**). The overall yield of TAL was ~0.11 g TAL per g glucose, and the overall production rate was 0.035 g L^{-1} h^{-1}. This experiment was repeated to produce additional TAL batches for bioTAL-PDK synthesis (**Supplementary Fig. 34**). Though unoptimized, these results compare favorably to previous TAL yields from mixed carbon sources (glucose, fructose, sucrose, and acetate) in *Rhodotorula toruloides* by 2-PS (0.089 g TAL per g mixed carbon sources).[41,42] After production and lyophilization of the broth, we extracted the mixture with ethyl acetate and isolated the desired TAL bioproduct (bioTAL) in high purity (**Supplementary Fig. 35**). We then synthesized a biorenewable triketone monomer bioTAL-TK **3** from bioTAL and sebacic acid, which we obtained as a bioproduct from Arkema. These 100% biorenewable triketone monomers showed essentially identical properties, when used in the synthesis and chemical recycling of bioTAL-PDK **3** resins (**Fig. 3d**).

LCA and TEA of TAL bioproduction

To understand the key cost and GHG emissions drivers of bioTAL production, we carried out a system-level techno-economic analysis (TEA) and life-cycle GHG inventory. All costs and emissions estimates are based on the system summarized in **Fig. 4a**. We modeled a biorefinery where corn stover is pretreated with a bio-compatible ionic liquid (cholinium lysinate), followed by enzymatic hydrolysis, to generate a hydrolysate, which can be converted to bioTAL via bioconversion of both pentose and hexose sugars in engineered *E. coli* expressing the non-native BktB thiolase. The cost of production is captured by a single metric minimum selling price (MSP). MSP refers to the product selling price at which the net present value of the project equals zero, after incorporating an internal rate of return (10% for this study). In other words, the MSP is the minimum price a company must sell the product for to be as profitable as their next best investment option. To estimate the MSP and generate mass and energy balances, we used a combination of experimental data and chemical process modeling to design and simulate a hypothetical commercial-scale bioTAL production facility. All process simulation was conducted in a commercial process modeling software package (SuperPro Designer-V12).[43] We translated outputs from the process model, including equipment sizing and costs, operating inputs, and waste processing costs, into a separate cash flow model to determine the MSP of bioTAL.

To understand the impact of bioTAL yield and other process parameters on MSP, we analyzed four biomass-derived bioTAL production scenarios based on the current demonstrated and future optimized yields. The scenario associated with "this work" reflects the bioTAL yield experimentally demonstrated in this study with glucose, extrapolated to xylose assuming a commercial-scale biorefinery would use a co-fermenting host. For comparison, we also considered a scenario built from the bioTAL yield in *R. toruloides* using 2-PS, as reported by Cao *et al.*[37] (**Fig. 4b**). The "intermediate" scenario extrapolates from this study with a moderate improvement upon the current bioTAL yield, reaching approximately 50% of the theoretical maximum (0.35 g bioTAL per g glucose, 0.315 g bioTAL per g xylose). Both "this work" and "intermediate" scenarios rely on a bioconversion residence time of approximately 75 h. An "optimized" scenario represents a mature facility in which the bioTAL yield reaches approximately 90% of theoretical maximum (0.63 g bioTAL per g glucose, 0.567 g bioTAL per g xylose) and all process parameters have been optimized to reach a practical minimum production cost, including a reduction in residence time to 48 h. Material balances for the intermediate scenario and major costs and

revenues associated with bioTAL production are presented in **Supplementary Tables 8 & 9**, respectively.

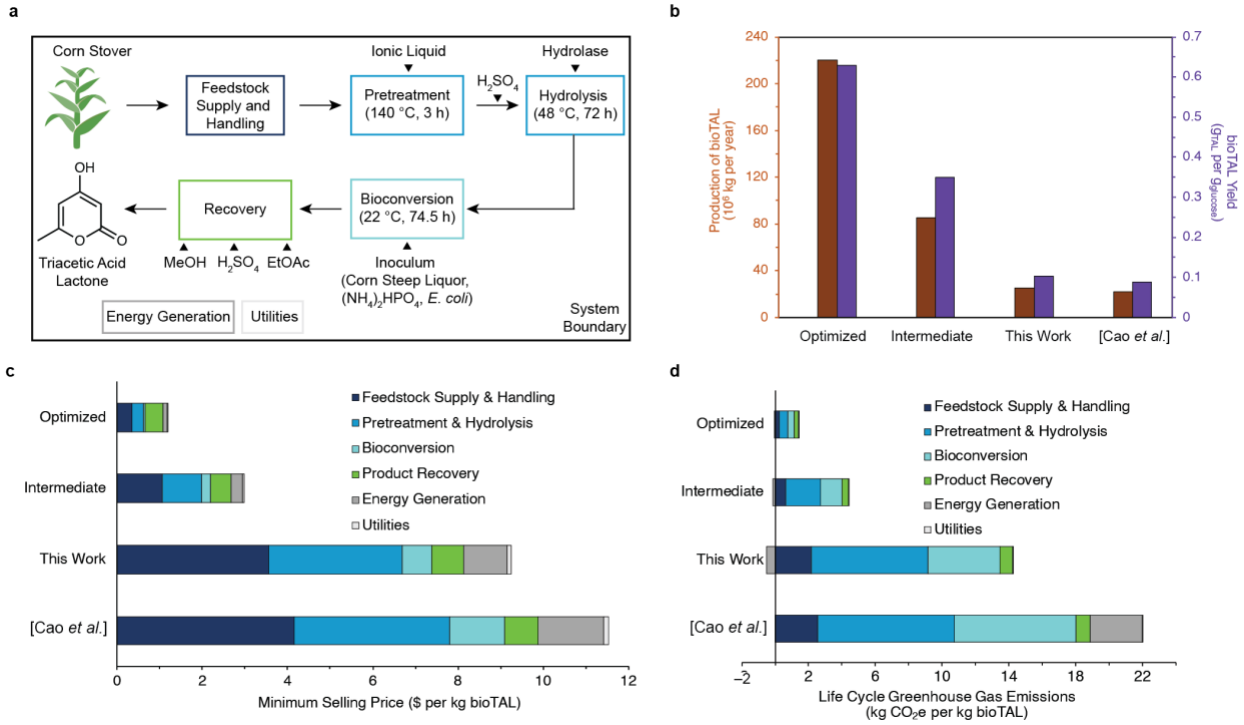

Fig. 4: Systems analysis of the production of bioTAL. a, Simplified schematic system boundary. **b**, bioTAL annual production and yield under four different scenarios, adjusting for factors such as the product yield (Cao *et al.*: 12.7% of theoretical maximum,[37] This Work: 14.9% of theoretical maximum, Intermediate: 50% of theoretical maximum, and Optimized: 90% of theoretical maximum) and projected efficiencies gained at industrial scale. **c**, Minimum selling price (MSP) and **d**, Life cycle GHG emissions for bioTAL production across all four scenarios.

In biorenewable PDK production, bioTAL serves as a replacement to dimedone, a petrochemical priced at $10 per kg.[44] As shown in **Fig. 4c**, all three scenarios tied to bioTAL production in *E. coli* using non-native BktB enzymes result in a lower MSP than the reported price for dimedone, whereas MSP is higher for the previously reported bioTAL production using 2-PS in *R. toruloides*. This encouraging result suggests that, provided the microbial host can be engineered to co-utilize both pentose and hexose sugars at comparable yields and rates, commercial-scale bioTAL production from corn stover can be cost-competitive with dimedone in the near term. The MSP results for the "optimized" scenario of approximately $2 per kg bioTAL represent a practical minimum and can be useful in screening for other applications where bioTAL may or may not compete with incumbent molecules. This optimized scenario can be viewed as something akin to a theoretical minimum; it is unlikely that costs could be reduced beyond that level. This exercise is useful because, if the optimized scenario were to result in higher costs than the petrochemical alternative (dimedone), this might suggest that bioTAL is not a viable replacement. For context, the price of HDPE, PU and PET is $2.3 per kg, $4 per kg, and $1.2 per kg, respectively.[45] Using the optimized scenario, replacing dimedone with bioTAL would result in a cost lower than the previously published PDK cost.[26] Improvements across all aspects of the production system, including lower-cost corn stover, improved sugar yields, higher ionic liquid recovery rates, and

increases in titer, rate, and yield are needed to reach this ambitious target. In the near-term, further research can improve the bioTAL recovery process (e.g., bioTAL refinement via recrystallization, instead of chromatography), which will improve both the costs and energy use.

The life-cycle GHG assessment is based on a cradle-to-gate system boundary and the functional unit is defined as one kg of bioTAL produced. We obtained life-cycle inventory data and characterization factors for input materials and commodity polymers from peer-reviewed literature,[25,46,47] and LCA databases including Ecoinvent,[48] US Life Cycle Inventory (USLCI),[49] GREET,[50] and WARM[51] models. The GHG emissions footprint for dimedone has been reported to be 0.7–15 kg CO_2e per kg dimedone in previous works.[26] To contextualize our results, we use a median value of 8 kg CO_2e per kg of dimedone. The intermediate and optimized scenarios in **Fig. 4d** result in lower GHG emissions compared to dimedone. This result is encouraging, as it suggests that even with moderate improvement in current bioTAL yield for the intermediate scenario, keeping all other assumptions constant, commercial-scale bioTAL production from corn stover can result in lower GHG emissions when compared to dimedone in the near term. GHG emissions are higher for the previously reported bioTAL production using 2-PS in *R. toruloides*, when compared to dimedone. For "this work" scenario, we found that GHG emissions is 1.7 times higher than the median value, and approximately equal to the highest reported value of dimedone.

Lower product yields and long bioconversion residence times translate into higher energy use, which drives GHG emissions. If lignin recovered from biomass is sufficient to meet the facility's heat and electricity demands, no fossil fuels are directly required. Any excess electricity can be sold to the grid (**Supplementary Table S10**); we assume these exports offset the U.S. average grid mix. If lignin is not sufficient, supplemental natural gas is required for on-site combined heat and power generation. We found for the bioTAL production reported in "this work" scenario that the pretreatment process is the single largest contributor to life cycle GHG emissions (51%), followed by bioconversion (31%). Switching to non-fossil energy sources could drive down the GHG footprint. Another opportunity for GHG emissions reduction would be to improve the solvent recovery rate. We assume 95% solvent recovery (ethyl acetate, methanol), which is readily achieved at industrial scale.

Discussion

Our summary findings show that biorenewable circularity with TAL-PDK is most promising when: bioprocesses for TAL production can be incorporated into lignocellulosic biorefineries that take in crop residues and other sustainable biomass feedstocks; engineered microorganisms metabolize both pentose and hexose sugars; and bioTAL yields are high. We also find that the high efficiency, low cost, and low-carbon intensity of PDK deconstruction and monomer recovery continues to stand out,[10–22] even among emerging circular plastics.[23–28] In particular, our use of TAL in place of petrochemicals in PDK production does not negatively impact PDK circularity. Instead, TAL provides an unexpected and useful bio-advantage with regard to the thermal behavior of TAL-PDK materials, which is exploited to expand the range of serviceable applications.

BioTAL production shows promise as a bio-advantaged alternative to dimedone in the formulation of biorenewable circular PDK resins. Even moderate improvements in yield can result in costs and

life-cycle GHG emissions that are more competitive with the incumbent petrochemicals currently used in PDK production. However, large-scale production will require advancements along the entire supply chain to enable more efficient utilization of corn stover, including high sugar yields, the use of microbial hosts capable of metabolizing pentose and hexose sugars, and improvements in bioTAL yields. In the future, we anticipate that synthetic biology will play an increasingly important role in PDK development. PDK properties can be tailored by an interplay of structure and chirality in monomer designs. A wide variety of structurally diverse diacids and 1,3-diketones (i.e., beyond TAL) are, in principle, accessible as polyketide bioproducts, offering new targets for bioproduction (e.g., by engineered polyketide synthases).[52] Depending on the process and the feedstock required, PDK sustainability may further benefit from these carbon-negative technologies.

Methods

Synthesis of Triketone Monomers

Triacetic acid lactone (2.1 eq), carboxylic diacid (1 eq), and dimethylaminopyridine (DMAP, 3 eq) were solubilized in tetrahydrofuran upon heating at 70 °C. A separate solution of dicyclohexylcarbodiimide (DCC, 2.4 eq) in tetrahydrofuran was added slowly to the reaction mixture. The reaction mixture gradually turned yellow, accompanied by the formation of a white precipitate. After the complete addition of DCC, the reaction was allowed to cool to room temperature and pursued overnight (24 h). The mixture was filtered and washed with CH_2Cl_2 until the solid became colorless. The filtrate was concentrated and the recovered product, a dark red oil, was dissolved in CH_2Cl_2 and extracted twice with 2.0 M HCl. The organic phase was dried over $MgSO_4$ and concentrated, leaving the crude product as an orange paste. The crude product was recrystallized from ethanol/water to yield yellow/orange needles.

Synthesis of PDK Resins

The polymerization of PDK resins was realized using ball-milling. To the triketone monomer was added *tris*(2-aminoethyl)amine (TREN) using a pre-calibrated micropipette such that the molar ratio of amine to triketone functional groups is 1.1 : 1. This was immediately followed by ball-milling the contents of the closed container for 30 min at 500 rpm with changes in spinning direction in 1-min intervals. The reactor was opened to air and the reactor walls were scraped to bring together the reactants homogeneously. Ball-milling was resumed under identical conditions for an additional 30 min. The powders were recovered from the reactor and the residual water was removed under vacuum at 90 °C.

Acid-Catalyzed Hydrolysis of PDK Samples

PDK materials were placed in separate 40 mL vials along with 5.0 M HCl (15 mL) and a magnetic stirrer. Depolymerization reactions were conducted over 24 h at room temperature while stirring at 500 rpm. Triketones were isolated by extraction with CH_2Cl_2 and evaporation of the organic phase.

Preparation of PDK Plastics for Hydrolysis

PDK resins obtained from ball-milling were compression-molded into sheets of ~ 1 mm in thickness using a thermal press operating at 110°C for TAL-PDK **5**, 125°C for TAL-PDK **4**, 130°C for TAL-PDK **3**, 140°C for TAL-PDK **2**, and 150°C for TAL-PDK **1** and 20,000 psi for 20 min. Small rectangular samples used for depolymerization studies were shaped with dimensions of l = 20 mm, w = 5 mm, t = 1 mm.

Fed-batch fermentation for TAL production

The strain used for TAL production is *E. coli* JBEI-3695 harboring plasmid pBbA5a-bktB (https://public-registry.jbei.org/entry/20892). A single colony of the strain was inoculated into 10 ml of LB medium and grown overnight at 37 ℃. This seed culture (1 mL) was inoculated into LB

(100 mL) in a 1-L shake flask and grown with shaking at 37 ℃ for 16 h, before inoculation into 1-L EZ-Rich medium (OD_{600} = 0.05) in a 2-L bioreactor (Sartorius BIOSTAT B plus). Agitation, temperature, airflow, and pH were maintained constant at 300 rpm, 22 ℃, 0.5 vvm and pH 7.0, respectively. The culture was grown for 3–4 h at 37 °C to OD_{600} = 0.6, at which point 0.1 mM IPTG was added to the culture to induce protein production. The temperature was adjusted to 22 ℃, and the culture was grown for 7 days. Fed-batch experiments employed a DO signal-triggered glucose feeding loop (ΔDO = 15 %, Flow rate = 40 mL h^{-1}, Pump duration = 5 min). 1 mL cell culture was removed every 24 h for cell density and TAL titer measurement. At the end of the 5-day culture, the cultures were harvested at 8,000 rpm, and TAL was extracted and purified from the supernatant.

System analysis of bioTAL production using SuperPro Model

The first step to conducting scenario analysis is establishing stoichiometrically maximum achievable yields. We calculated the stoichiometric maximum theoretical yield of bioTAL from glucose to be 0.7 g per g glucose. For all four scenarios considered in this study, we assumed xylose to bioTAL conversion to be 90% of that of glucose to bioTAL conversion. The scenario associated with "this work" reflects the bioTAL yield experimentally demonstrated in this study with glucose (14.9% of theoretical maximum yield), extrapolated to xylose assuming a commercial-scale biorefinery would use a co-fermenting host. A 2.6 g L^{-1} titer was used to calculate the yield in glucose (0.104 g g^{-1} glucose). Then, assuming xylose to bioTAL conversion to be 90% of that of glucose to bioTAL conversion, the yield from xylose to bioTAL conversion was also calculated. A 2.6 g L^{-1} titer was used for the modeling purpose (instead of the highest reported titer of 2.77 g L^{-1}) as at 2.6 g L^{-1}, the temperature of the bioconversion units could be kept lower, which reduces the energy use of the system significantly, and thus lowers the MSP and the GHG emissions of the system. The intermediate and optimized scenario are based on the assumption of achieving 50% and 90% of theoretical yield based on glucose, respectively. The "Cao *et al.*" scenario is based on the bioTAL yield information obtained from article mentioned here (12.7% of theoretical maximum yield).[37]

We conducted the process modeling in SuperPro Designer software.[43] The biorefinery operates 330 days per year and 24 h per day (equivalent to 90% uptime). Capital cost accounts for equipment purchase cost, installation costs, warehouse, site development, permits, land, and other field expenses and project contingency costs. Annual operating cost accounts for materials, utilities, repair and maintenance, labor, and waste disposal costs. The assumptions for the model are consistent with Humbird *et al.* unless otherwise specified.[53] The bulk prices for material costs were obtained from peer-reviewed literature, market price reports, and Alibaba. Equipment purchase prices were derived using built-in cost estimating function available in SuperPro. The process parameters and assumptions for "this work" and optimized scenarios are summarized in **Supplementary Table 11**. With the exception of yield, all other process parameters remained the same for "this work" and intermediate scenarios. For the Cao *et al*. scenario, the same assumptions and parameters were used as that in "this work" scenario, except during bioconversion where we used a residence time and temperature of 120 h and 30 °C, respectively, and during the recovery process, where we used crystallization to recover bioTAL instead of column chromatography. [37]

Data Availability

The authors declare that the data supporting the findings of this study are available within the paper and its Supplementary Information. Crystallographic data for compounds TAL-TK **1**, TAL-TK **3** and TAL-TK **5** are available free of charge from the Cambridge Crystallographic Data Centre (www.ccdc.cam.ac.uk) under reference numbers 2223455, 2223456 and 2223457, respectively.

Acknowledgments

We acknowledge support from the U.S. Department of Energy (DOE) Bioenergy Technologies Office award number 1916-1597. Portions of this work—including polymer synthesis, recycling, and characterization—were carried out as a User Project at the Molecular Foundry, which is supported by the Office of Science, Office of Basic Energy Sciences, of the U.S. Department of Energy under Contract No. DE-AC02-05CH11231. This work was supported by Joint BioEnergy Institute (https://www.jbei.org), which is supported by the DOE, Office of Science, Office of Biological and Environmental Research under contract DE-AC02-05CH11231. This Solid-State NMR instrument used in this work is supported by the National Science Foundation under Grant No. 2018784. This research used resources of the Advanced Light Source, which is a DOE Office of Science User Facility under contract no. DE-AC02-05CH11231. We thank Dr. A. Lund for her help with the solid-state NMR data acquisition. We thank S.L. Nordahl for helpful discussions on LCA analysis.

Author Contributions Statement

All authors contributed to the conceptualization of the project. J.D., B.C. and B.A.H. contributed the methodology for polymer design and chemical recycling. B.B., N.R.B., and C.D.S contributed the methodology for systems analysis. Z.W., S.C., G.L. and J.D.K. contributed the methodology for bioTAL production. S.J.T. contributed the methodology for monomer characterization by X-ray diffraction. All authors contributed to analyzing the data. B.A.H., J.D., Z.W., and B.B. wrote the original draft. All authors contributed to writing the final draft and editing. B.A.H. and J.D. contributed to visualization. B.A.H. supervised the research. J.D.K., C.D.S. and B.A.H. provided project administration. J.D.K., C.D.S. and B.A.H. acquired funding.

Competing Interests Statement

The authors declare the following competing interests: B.A.H. is an inventor on the U.S. provisional patent application 62/587,148 submitted by Lawrence Berkeley National Laboratory that covers PDKs, as well as aspects of their use and recovery. B.A.H., J.D. and J.D.K. are inventors on the U.S. provisional patent application 63/390,962 submitted by Lawrence Berkeley National Laboratory that covers TAL-PDKs, as well as aspects of their use and recovery. J.D.K. has a financial interest in Amyris, Lygos, Demetrix, Napigen, Maple Bio, Apertor Labs, Berkeley Yeast, Ansa Biotechnologies, and Zero Acre Farms. B.A.H., J.D.K., and C.D.S. have a financial interest in Cyklos Materials. The other authors declare that they have no other competing interests.

References

1. Rosenboom, J.-G., Langer, R. & Traverso, G. Bioplastics for a circular economy. *Nat. Rev. Mater.* **7**, 117–137 (2022).
2. Kakadellis, S. & Rosetto, G. Achieving a circular bioeconomy for plastics. *Science* **373**, 49–50 (2021).
3. Fagnani, D. E. et al. 100th Anniversary of Macromolecular Science Viewpoint: Redefining Sustainable Polymers. *ACS Macro Lett.* **10**, 41–53 (2021).
4. Haque, F. M. *et al.* Defining the Macromolecules of Tomorrow through Synergistic Sustainable Polymer Research. *Chem. Rev.* **122**, 6322–6373 (2022).
5. Kawaguchi, H., Ogino, C. & Kondo, A. Microbial conversion of biomass into bio-based polymers. *Bioresour. Technol.* **245**, 1664–1673 (2017).
6. Cywar, R. M., Rorrer, N. A., Hoyt, C. B., Beckham, G. T. & Chen, E. Y.-X. Bio-based polymers with performance-advantaged properties. *Nat. Rev. Mater.* **7**, 83–103 (2022).
7. Coates, G. W. & Getzler, Y. D. Y. L. Chemical recycling to monomer for an ideal, circular polymer economy. *Nat. Rev. Mater.* **5**, 501–516 (2020).
8. Borrelle, S. B. *et al.* Predicted growth in plastic waste exceeds efforts to mitigate plastic pollution. *Science* **369**, 1515–1518 (2020).
9. von Vacano, B. *et al.* Sustainable Design of Structural and Functional Polymers for a Circular Economy. *Angew. Chem. Int. Ed.* **62**, e202210823 (2022).
10. Haeussler, M., Eck, M., Rothauer, D. & Mecking, S. Closed-loop recycling of polyethylene-like materials. *Nature* **590**, 423–427 (2021).
11. Abel, B. A., Snyder, R. L. & Coates, G. W. Chemically recyclable thermoplastics from reversible-deactivation polymerization of cyclic acetals. *Science* **373**, 783–789 (2021).
12. Rapagnani, R. M., Dunscomb, R. J., Fresh, A. A. & Tonks, I. A. Tunable and recyclable polyesters from CO_2 and butadiene. *Nat. Chem.* **14**, 877–883 (2022).
13. Zhu, J.-B., Watson, E. M., Tang, J. & Chen, E. Y.-X. A synthetic polymer system with repeatable chemical recyclability. *Science* **360**, 398–403 (2018).
14. Hong, M. & Chen, E. Y.-X. Completely recyclable biopolymers with linear and cyclic topologies via ring-opening polymerization of γ-butyrolactone. *Nat. Chem.* **8**, 42–49 (2016).
15. Cywar, R. M. *et al.* Redesigned Hybrid Nylons with Optical Clarity and Chemical Recyclability. *J. Am. Chem. Soc.* **144**, 5366–5376 (2022).
16. Yuan, P., Sun, Y., Xu, X., Luo, Y. & Hong, M. Towards high-performance sustainable polymers via isomerization-driven irreversible ring-opening polymerization of five-membered thionolactones. *Nat. Chem.* **14**, 294–303 (2022).
17. Lei, Z. *et al.* Recyclable and malleable thermosets enabled by activating dormant dynamic linkages. *Nat. Chem.* **14**, 1399–1404 (2022).
18. Mohadjer Beromi, M. *et al.* Iron-catalysed synthesis and chemical recycling of telechelic 1,3-enchained oligocyclobutanes. *Nat. Chem.* **13**, 156–162 (2021).
19. Zhang, Z. *et al.* Strong and Tough Supramolecular Covalent Adaptable Networks with Room-Temperature Closed-Loop Recyclability. *Adv. Mater.* **35**, 2208619 (2022).
20. Sullivan, K. P. *et al.* Mixed plastics waste valorization through tandem chemical oxidation and biological funneling. *Science* **378**, 207–211 (2022).
21. Saito, K., Eisenreich, F., Tuerel, T. & Tomovic, Z. Closed-Loop Recycling of Poly(Imine-Carbonate) Derived from Plastic Waste and Bio-based Resources. *Angew. Chem. Int. Ed.* **61**, e202211806 (2022).
22. Li, Z., Zhao, D., Shen, Y. & Li, Z. Ring-opening Polymerization of Enantiopure Bicyclic Ether-ester Monomers toward Closed-loop Recyclable and Crystalline Stereoregular Polyesters via Chemical Upcycling of Bioplastic. *Angew. Chemie Int. Ed.* **n/a**, e202302101 (2023).
23. Christensen, P. R., Scheuermann, A. M., Loeffler, K. E. & Helms, B. A. Closed-loop recycling of plastics enabled by dynamic covalent diketoenamine bonds. *Nat. Chem.* **11**, 442–448 (2019).

24. He, C. *et al.* Conformational Entropy as a Means to Control the Behavior of Poly(diketoenamine) Vitrimers In and Out of Equilibrium. *Angew. Chem., Int. Ed.* **59**, 735–739 (2020).
25. Vora, N. *et al.* Leveling the cost and carbon footprint of circular polymers that are chemically recycled to monomer. *Sci. Adv.* **7**, eabf0187 (2022).
26. Demarteau, J., Vora, N., Keasling, J. D., Helms, B. A. & Scown, C. D. Lower-Cost, Lower-Carbon Production of Circular Polydiketoenamine Plastics. *ACS Sustain. Chem. Eng.* **10**, 2740–2749 (2022).
27. Demarteau, J. *et al.* Circularity in mixed-plastic chemical recycling enabled by variable rates of polydiketoenamine hydrolysis. *Sci. Adv.* **8**, eabp8823 (2022).
28. Helms, B. A. Polydiketoenamines for a Circular Plastics Economy. *Acc. Chem. Res.* **55**, 2753–2765 (2022).
29. Vermeulen, I., Van Caneghem, J., Block, C., Baeyens, J. & Vandecasteele, C. Automotive shredder residue (ASR): Reviewing its production from end-of-life vehicles (ELVs) and its recycling, energy or chemicals' valorization. *J. Hazard. Mater.* **190**, 8–27 (2011).
30. Denissen, W., Winne, J. M. & Du Prez, F. E. Vitrimers: permanent organic networks with glass-like fluidity. *Chem. Sci.* **7**, 30–38 (2016).
31. Jin, Y.; Lei, Z.; Taynton, P.; Huang, S.; Zhang, W. Malleable and Recyclable Thermosets: The Next Generation of Plastics. *Matter* **1**, 1456−1493 (2019).
32. Scheutz, G. M.; Lessard, J. J.; Sims, M. B.; Sumerlin, B. S. Adaptable Crosslinks in Polymeric Materials: Resolving the Intersection of Thermoplastics and Thermosets. *J. Am. Chem. Soc.* **141**, 16181−16196 (2019).
33. Wang, R., Johnson, J. A. & Olsen, B. D. Odd-Even Effect of Junction Functionality on the Topology and Elasticity of Polymer Networks. *Macromolecules* **50**, 2556–2564 (2017).
34. Coffman, D. D., Berchet, G. J., Peterson, W. R. & Spanagel, E. W. Polymeric amides from diamines and dibasic acids. *J. Polym. Sci.* **2**, 306–313 (1947).
35. Rimando, A, Baerson, S. Polyketides: Biosynthesis, Biological Activity, and Genetic Engineering. *Polyketides (ACS Symposium Series)* **955**, 1–5 (2007).
36. Markham, K. A. *et al.* Rewiring Yarrowia lipolytica toward triacetic acid lactone for materials generation. *Proc. Natl. Acad. Sci. U. S. A.* **115**, 2096–2101 (2018).
37. Cao, M. *et al.* Metabolic engineering of oleaginous yeast *Rhodotorula toruloides* for overproduction of triacetic acid lactone. *Biotechnol. Bioeng.* **119**, 2529–2540 (2022).
38. Tan, Z., Clomburg, J. M., Cheong, S., Qian, S. & Gonzalez, R. A polyketoacyl-CoA thiolase-dependent pathway for the synthesis of polyketide backbones. *Nat. Catal.* **3**, 593–603 (2020).
39. Wang, Z. *et al.* A highly active Burkholderia polyketoacyl-CoA thiolase for production of triacetic acid lactone. *BioRxiv* doi: 10.1101/2022.12.04.519061 (2022).
40. Sierra-Ibarra, E. *et al.* Ethanol production by *Escherichia coli* from detoxified lignocellulosic teak wood hydrolysates with high concentration of phenolic compounds. *J. Ind. Microbiol. Biotechnol.* **49**, kuab077 (2022).
41. Tang, S.-Y. *et al.* Screening for Enhanced Triacetic Acid Lactone Production by Recombinant Escherichia coli Expressing a Designed Triacetic Acid Lactone Reporter. *J. Am. Chem. Soc.* **135**, 10099–10103 (2013).
42. Xie, D. *et al.* Microbial synthesis of triacetic acid lactone. *Biotechnol. Bioeng.* **93**, 727–736 (2006).
43. SuperPro Designer, Scotch Plains, NJ, 2014.
44. September 2022 value from Website: https://www.alibaba.com/product-detail/CAS-126-81-8-Dimedone-C8H12O2_1600455883706.html?spm=a2700.7724857.0.0.79e37b39MEK2Ha.
45. Feb 2023 values from Website: a) https://www.alibaba.com/product-detail/Granules-Hdpe-Factory-Price-Pipe-Grade_1600284744902.html?spm=a2700.galleryofferlist.0.0.142858bcBUPNVJ; b) https://www.alibaba.com/product-detail/High-Quality-China-Manufacture-Foaming-Agent_1600661087016.html?spm=a2700.7724857.0.0.60448b57efKUZa&s=p; c) https://www.alibaba.com/product-detail/Pet-Resin-Polyethylene-Terephthalate-Plastic-Raw_1600190831818.html?spm=a2700.details.0.0.67cd6493D58qSL.

46. Amelio, A., Genduso, G., Vreysen, S., Luis, P. & der Bruggen, B. Guidelines based on life cycle assessment for solvent selection during the process design and evaluation of treatment alternatives. *Green Chem.* **16**, 3045–3063 (2014).
47. Kyulavska, M., Toncheva-Moncheva, N. & Rydz, J. Biobased Polyamide ecomaterials and their susceptibility to biodegradation. *Handb. Ecomater.* (Springer, 2017).
48. Wernet, G. *et al.* The ecoinvent database version 3 (part I): overview and methodology. *Int. J. Life Cycle Assess.***21**, 1218–1230 (2016).
49. National Renewable Energy Laboratory, *US Life Cycle Inventory Database* (2012); http://www.nrel.gov/lci/.
50. Wang, M. *et al.* GREET Model: The Greenhouse Gases, Regulated Emissions, and Energy Use in Transportation Model. (2014).
51. Warm, E. Waste Reduction Model. *US Environ. Prot. Agency Washington, DC* (2010).
52. Huang Y, Hoefgen S, Gherlone F, Valiante V. Intrinsic ability of the β-Oxidation pathway to produce bioactive styrylpyrones. *Angew. Chem. Int. Ed.* **61**, e202206851 (2022).
53. Humbird, D. *et al. Process Design and Economics for Biochemical Conversion of Lignocellulosic Biomass to Ethanol: Dilute-Acid Pretreatment and Enzymatic Hydrolysis of Corn Stover*. http://www.osti.gov/servlets/purl/1013269-rQta8H/ (2011) doi:10.2172/1013269.